Journal of Sound and Vibration (1999) **223**(4), 645–657
Article No. jsvi.1999.2154, available online at http://www.idealibrary.com on IDEAL®

TIPPING LOADS OF MOBILE CRANES WITH FLEXIBLE BOOMS

S. KILIÇASLAN, T. BALKAN AND S. K. IDER
Department of Mechanical Engineering, Middle East Technical University, 06531 *Ankara, Turkey*

(*Received* 23 *July* 1997, *and in final form* 4 *January* 1999)

In this study the characteristics of a mobile crane are obtained by using a flexible multibody dynamics approach, for the determination of safe loads to prevent tipping of a mobile crane. Only the boom of the crane is assumed to be flexible since it is the only element that has considerable deflections in applications. The coupled rigid and elastic motions of the crane are formulated and software is developed in order to carry out the dynamic analysis. The variation of piston force with respect to boom angular position for different boom motion times are simulated, load curves are generated and the results are compared with the experimental results obtained from a 10 t mobile crane.

1. INTRODUCTION

Cranes as mechanical systems are in general closed-chain mechanisms with flexible members. In the problem of determination of safe loads which as a function of the boom angular position, the solution of the dynamic equations is necessary.

There are few studies related to the dynamics and control of mobile cranes for various applications. In almost all of these studies the body flexibility is not taken into consideration. A dynamic model for the control of a flexible rotary crane which carries out three kinds of motion (rotation, load hoisting and boom hoisting) simultaneously is derived by Sato and Sakawa [1]. Only the joint between the boom and the jib is assumed to be flexible. The goal is to transfer a load to a desired place in such a way that at the end of the transfer the swing of the load decays as quickly as possible. The application of a hook load and safe load indicator and limiter for mobile cranes is presented by Balkan where the microprocessor-based control system for the determination of current hook load is based on oil pressure and boom angle [2].

In this paper, mobile crane characteristics are determined by using flexible multibody analysis. Kinematics and equations of motion of the flexible multibody system are derived. Software has been developed to carry out dynamic analysis of the crane. In the flexible dynamic analysis, the coupled rigid and elastic motion of the system is formulated by using absolute co-ordinates

0022–460X/99/240645 + 13 $30.00/0

and modal variables [3, 4]. Then, joint connections and prescribed motions are imposed as constraint equations. The flexible body is modelled by the finite element method and modal variables are used as the elastic variables by utilizing modal transformation.

The variations of the piston force with respect to the boom angular positions are analyzed for different boom motion times to illustrate the effect of flexibility by using the developed software. Load curves are generated for various boom motion times and compared to those of the manufacturer.

2. MODELLING OF THE CRANE

Since there is experimental work on the tipping load control of a COLES Mobile 930 crane, for the application of the developed software, the structure of the above mentioned crane and its parameters are used [5]. However, the method of analysis can easily be applied to similar types of cranes with simple modifications.

In general, mobile cranes are operated under blocked conditions by the vertical jacks. The load is attached to the hook and the boom is hoisted. Since the excessive raising of the load is dangerous, the height of the load is controlled by lengthening the rope. During hoisting, lowering and transportation of the load, the crane is not rotated, due to some restrictions such as very huge and/or heavy loads, space problems, etc.

In every angular position of the boom, there is a maximum load above which tipping might probably occur. Since the angular position of the boom changes only during the up and down motion of the load, which is actually a planar motion, modelling and analysis are carried out in two dimensions.

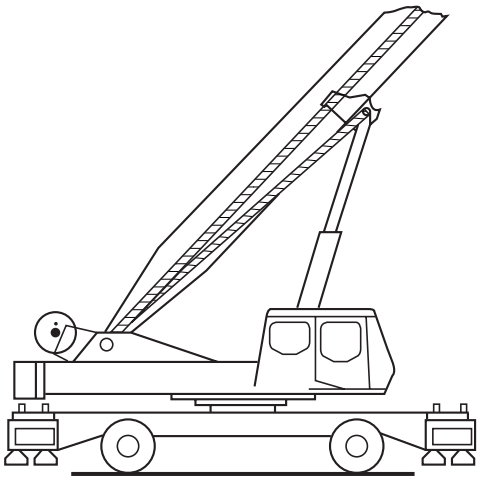

Figure 1. Schematic representation of the test crane.

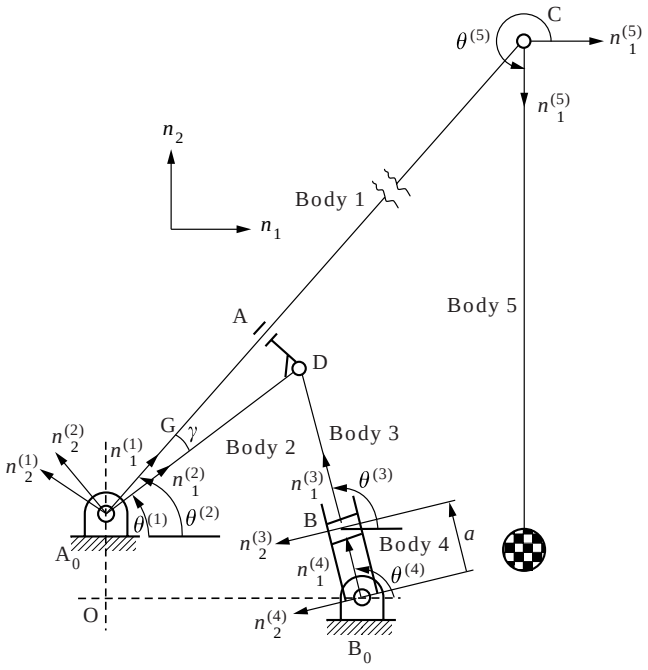

Figure 2. Kinematic model of the test crane. Dimensions in mm: A_0G 2000; GC 17 500; A_0A 5823; A_0D 5850; AD 565; BD 3455; OB_0 2350; OA_0 805.

Schematic representation of the test crane is shown in Figure 1 and the kinematic model of the test crane which can be represented by five bodies is shown in Figure 2.

Cross-section, material properties and dimensions of each body are obtained from the technical data sheet and measured directly from the test crane. The cross-section of Body 1 is a hollow polygon of thickness, t, as shown in Figure 3. The cross-section dimensions increase from A_0 to G and decrease from G to C linearly, and the dimensions at sections A_0, G and C are shown in Figure 3. Body 2 is a cylindrical rod 25 mm in diameter and Body 3 is a piston 180 mm in

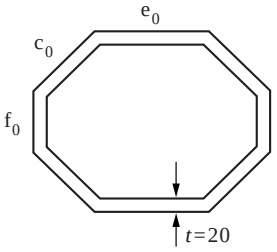

	A_0	G	C
e_0	453	160	160
c_0	200	440	207
f_0	120	120	120

Figure 3. Cross-section of Body 1. Dimensions in mm.

diameter with spool thickness of 20 mm. Body 4 is a cylinder with inner diameter of 230 mm, outer diameter of 246 mm and length of 3440 mm. Additionally, modulus of elasticity and mass density of the Body 1 are taken as 200 GPa and 5750 kg/m^3, respectively. Mass density of other bodies are taken as 7850 kg/m^3.

When dimensions (lengths and cross-sections) and elastic properties of the bodies of the crane are considered, it is sufficient to take only the Body 1 (the boom) as flexible. In this case, other bodies are assumed to be rigid.

The following assumptions are considered in the analysis of the crane.

1. The mass of the hydraulic oil is included in the mass of the cylinder (Body 4). Varying mass of the cylinder due to varying amounts of hydraulic oil inside it is taken into consideration.
2. Hydraulic oil is assumed incompressible.
3. The hook load is considered as a point mass and connected to the end of the boom with a rope which is taken as a rigid rod. This rope is free for planar rotation about point C. This assumption is valid as long as the oscillations of the rod about the vertical position are small and the rod remains in tension. These conditions are satisfied for normal operation speeds and hook loads.
4. The structural damping of the boom is taken into account by assuming Rayleigh damping.
5. The distance between the load and the base is assumed to be kept constant by varying the length of the rope during the up and down motion of the crane.

3. DYNAMIC EQUATIONS

Let n^k represent a body reference frame relative to which the deformation of Body k is defined and n represent a fixed frame. Let $\boldsymbol{\xi}^k$ represent the position of the origin Q of n^k in n, and $\boldsymbol{\omega}^k$ be the angular velocity of Body k.

Using the finite element method, the deformation displacement vector $\mathbf{u}^{ki}$ of an arbitrary point P in element i of Body k is

$$\mathbf{u}^{ki} = \boldsymbol{\phi}^{ki}\mathbf{B}^{ki}\boldsymbol{\alpha}^k \tag{1}$$

where $\boldsymbol{\phi}^{ki}$ is the element shape function matrix transformed to n^k, $\mathbf{B}^{ki}$ is the element connectivity Boolean matrix and $\boldsymbol{\alpha}^k$ is the vector of body nodal variables.

The velocity of P is written as

$$\mathbf{v}^{ki} = \dot{\boldsymbol{\xi}}^k + \mathbf{T}^k\tilde{\mathbf{q}}^{ki}\bar{\boldsymbol{\omega}}^k + \mathbf{T}^k\boldsymbol{\phi}^{ki}\mathbf{B}^{ki}\boldsymbol{\chi}^k\dot{\boldsymbol{\eta}}^k, \tag{2}$$

where $\mathbf{q}^{ki}$ is the position vector from Q to P in n^k including deformation, $\tilde{\mathbf{q}}^{ki}$ is the skew symmetric matrix of $\mathbf{q}^{ki}$, $\mathbf{T}^k$ is the co-ordinate transformation from n^k to n, $\bar{\boldsymbol{\omega}}^k = \mathbf{T}^{ki^T}\boldsymbol{\omega}^k$, $\boldsymbol{\chi}^k$ is modal transformation used to reduce the elastic degrees of freedom, and $\boldsymbol{\eta}^k$ is the vector of body modal variables. Equation (2) can be expressed as

$$\mathbf{v}^{ki} = \boldsymbol{\nu}^{ki}\mathbf{y}^k, \tag{3}$$

where $\mathbf{y}_T^{ki} = [\mathbf{I}\ \mathbf{T}^k\tilde{\mathbf{q}}^{ki}\ \mathbf{T}^k\boldsymbol{\phi}^{ki}\mathbf{B}^{ki}\boldsymbol{\chi}^k]$ is the influence coefficient matrix, and $\mathbf{y}^{k^T} = [\dot{\boldsymbol{\xi}}^{k^T}\ \bar{\boldsymbol{\omega}}^{k^T}\ \dot{\boldsymbol{\eta}}^{k^T}]$ is the vector of generalized speeds of Body k.

The joint connections and prescribed motions in the system of N interconnected bodies are represented by kinematic constraint equations expressed at velocity level as

$$\mathbf{C}\mathbf{y} = \mathbf{g}, \tag{4}$$

where $\mathbf{y}$ is the system generalized speed vector given by

$$\mathbf{y}^T = [\mathbf{y}^{(1)^T} \quad \cdots \quad \mathbf{y}^{(N)^T}]. \tag{5}$$

$\mathbf{C}$ is the constraint Jacobian matrix which can be formed by the velocity influence coefficient matrices and $\mathbf{g}$ indicates the prescribed velocities.

Kane's equations are used to determine the equations of motion of the system as

$$\mathbf{M}\dot{\mathbf{y}} + \mathbf{C}^T\boldsymbol{\lambda} = \mathbf{Q} + \mathbf{F}^s + \mathbf{F}^d + \mathbf{F}. \tag{6}$$

where $\boldsymbol{\lambda}$ is the vector of constraint forces, $\mathbf{M}$ is the generalized mass matrix, $\mathbf{Q}$, $\mathbf{F}^s$, $\mathbf{F}^d$ and $\mathbf{F}$ are vectors of Coriolis forces, elastic forces, damping forces and applied forces, respectively and

$$\mathbf{M} = \begin{bmatrix} \mathbf{M}^{(1)} & & \mathbf{0} \\ & \ddots & \\ \mathbf{0} & & \mathbf{M}^{(N)} \end{bmatrix}, \quad \mathbf{Q} = \begin{bmatrix} \mathbf{Q}^{(1)} \\ \vdots \\ \mathbf{Q}^{(N)} \end{bmatrix}, \quad \mathbf{F}^s = \begin{bmatrix} \mathbf{F}^{s^{(1)}} \\ \vdots \\ \mathbf{F}^{s^{(N)}} \end{bmatrix},$$

$$\mathbf{F}^d = \begin{bmatrix} \mathbf{F}^{d^{(1)}} \\ \vdots \\ \mathbf{F}^{d^{(N)}} \end{bmatrix}, \quad \mathbf{F} = \begin{bmatrix} \mathbf{F}^{(1)} \\ \vdots \\ \mathbf{F}^{(N)} \end{bmatrix}. \tag{7}$$

The mass matrix $\mathbf{M}^k$ and Coriolis vector $\mathbf{Q}^k$ of Body k are found as

$$\mathbf{M}^k = \sum_{i=1}^{E_k} \int_{V_{ki}} \rho_{ki}\mathbf{v}^{ki^T}\mathbf{v}^{ki}\,\mathrm{d}V, \tag{8}$$

and

$$\mathbf{Q}^k = -\sum_{i=1}^{E_k} \int_{V_{ki}} \rho_{ki}\mathbf{v}^{ki^T}(\dot{\mathbf{v}}^{ki}\mathbf{y}^k)\,\mathrm{d}V, \tag{9}$$

where E_k is the number of finite elements in Body k, V_{ki} is the volume of the ith element and ρ_{ki} is its mass density.

$\mathbf{F}^{s^k}$ and $\mathbf{F}^{d^k}$ can be written according to the generalized co-ordinate partitioning as

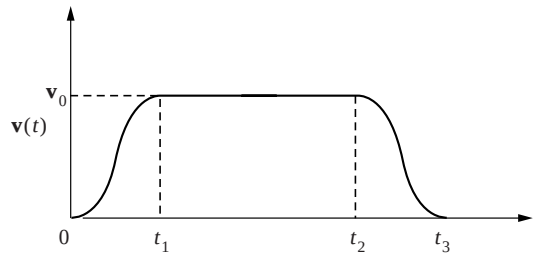

Figure 4. Velocity profile with cycloidal acceleration and deceleration.

$$\mathbf{F}^{s^k} = -\begin{bmatrix} \mathbf{0} \\ \mathbf{0} \\ \boldsymbol{\chi}^{k^T}\mathbf{K}^k\boldsymbol{\chi}^k\boldsymbol{\eta}^k \end{bmatrix}, \quad \mathbf{F}^{d^k} = -\begin{bmatrix} \mathbf{0} \\ \mathbf{0} \\ \boldsymbol{\chi}^{k^T}\mathbf{D}^k\boldsymbol{\chi}^k\dot{\boldsymbol{\eta}}^k \end{bmatrix}, \tag{10}$$

where $\mathbf{K}^k$ is the structural stiffness matrix and $\mathbf{D}^k$ is the structural Rayleigh damping matrix of Body k. In the simulations, the weights of the structural mass and stiffness matrices used in forming $\mathbf{D}^k$ correspond to a 2% damping ratio.

In a planar system $\mathbf{y}^k$ reduces to $\mathbf{y}^{k^T} = [\dot{\boldsymbol{\xi}}^{k^T}\ \dot{\theta}^k\ \dot{\boldsymbol{\eta}}^{k^T}]$ where $\dot{\theta}^k$ is a scalar and $\boldsymbol{\nu}^{ki}$ becomes $\boldsymbol{\nu}^{ki} = [\mathbf{I}\ \ \mathbf{T}^k_\theta\mathbf{q}^{ki}\ \ \mathbf{T}^k\boldsymbol{\phi}^{ki}\mathbf{B}^{ki}\boldsymbol{\chi}^k]$ where $\mathbf{T}^k_\theta$ is the derivative of $\mathbf{T}^k$ with respect to θ^k.

When the space dependent terms in equations (8) and (9) are separated, a set of time invariant matrices are obtained [3, 4]. These mass properties are evaluated once in advance. Equation (6) and the derivative of equation (4) represent linear equations for the accelerations $\dot{\mathbf{y}}$ and the constraint forces $\boldsymbol{\lambda}$. The accelerations obtained from these equations are numerically integrated by using a variable step, variable order predictor–corrector algorithm to obtain the time history of the generalized speeds and generalized co-ordinates.

The boundary conditions used for the description of the deformation of Body 1 are that for axial deformation A_0 is fixed, and for bending A_0 is hinged and A is fixed. The first axial mode, the first bending mode of part $\overline{A_0A}$ and the first two bending modes of part $\overline{AC}$ of Body 1 are taken as the modal co-ordinates since the higher modes are observed negligible. Therefore the generalized speed vector of the system is

$$\mathbf{y}^T = [\dot{\boldsymbol{\xi}}^{(1)^T}\ \ \dot{\theta}^{(1)}\ \ \dot{\boldsymbol{\eta}}^{(1)^T}\ \ \dot{\boldsymbol{\xi}}^{(2)^T}\ \ \dot{\theta}^{(2)}\ \ \dot{\boldsymbol{\xi}}^{(3)^T}\ \ \dot{\theta}^{(3)}\ \ \dot{\boldsymbol{\xi}}^{(4)^T}\ \ \dot{\theta}^{(4)}\ \ \dot{\boldsymbol{\xi}}^{(5)^T}\ \ \dot{\theta}^{(5)}], \tag{11}$$

where $\boldsymbol{\eta}^{(1)^T} = [\eta_1^{(1)}\ \eta_2^{(1)}\ \eta_3^{(1)}\ \eta_4^{(1)}]$ and $\boldsymbol{\xi}^{(k)^T} = [\xi_1^{(k)}\ \xi_2^{(k)}]$, $k = 1, \ldots, 5$.

The joint connection and prescribed motion constraints of equation (4) are:

(1) *The double revolute joints at* A_0 *and the revolute joint at* B_0:

$$\dot{\xi}_1^{(1)} = 0, \quad \dot{\xi}_2^{(1)} = 0, \quad \dot{\xi}_1^{(2)} = 0, \quad \dot{\xi}_2^{(2)} = 0, \quad \dot{\xi}_1^{(4)} = 0, \quad \dot{\xi}_2^{(4)} = 0. \tag{12}$$

(2) *The sliding joint at point* A:

$$\mathbf{T}_2^{\mathrm{A}}(\dot{\boldsymbol{\xi}}^{(1)} + \mathbf{T}_\theta^{(1)}\boldsymbol{\phi}^{\mathrm{A}_1}\mathbf{B}^{1p}\mathbf{e}^{(1)}\dot{\theta}^{(1)} + \mathbf{T}^{(1)}\boldsymbol{\phi}^{\mathrm{A}_1}\boldsymbol{\chi}^{(1)}\dot{\boldsymbol{\eta}}^{(1)} - \dot{\boldsymbol{\xi}}^{(2)} - \mathbf{T}_\theta^{(2)}\mathbf{r}^{\mathrm{A}_2}\dot{\theta}^{(2)}) = 0, \tag{13}$$

$$\dot{\theta}^{(1)} + \boldsymbol{\psi}^{A_1}\mathbf{B}^{1p}\boldsymbol{\chi}^{(1)}\dot{\boldsymbol{\eta}}^{(1)} - \dot{\theta}^{(2)} = 0. \tag{14}$$

Here $\boldsymbol{\phi}^{A_1}$ and $\boldsymbol{\psi}^{A_1}$ are respectively the deformation displacement and rotation shape functions of element p (which is the element that contains A_1) evaluated at point A_1, $\mathbf{e}^{(1)}$ is the vector of nodal variables of Body 1 including position coordinates of the nodal points, $\mathbf{r}^{A_2}$ is the local position vector of point A in frame $n^{(2)}$, and $\mathbf{T}_2^A = [-\sin(\theta^{(2)} + \gamma) \quad \cos(\theta^{(2)} + \gamma)]$ is the second row of the appropriate transformation matrix.

(3) *The revolute joint at point* D:

$$\dot{\boldsymbol{\xi}}^{(2)} + \mathbf{T}_\theta^{(2)}\mathbf{r}^{D_2}\dot{\theta}^{(2)} - \dot{\boldsymbol{\xi}}^{(3)} - \mathbf{T}_\theta^{(3)}\mathbf{r}^{D_3}\dot{\theta}^{(3)} = 0. \tag{15}$$

(4) *The sliding joint at point* B:

$$\dot{\theta}^{(3)} - \dot{\theta}^{(4)} = 0, \quad \mathbf{T}_2^B(\dot{\boldsymbol{\xi}}^{(3)} - \dot{\boldsymbol{\xi}}^{(4)} + \mathbf{T}_\theta^{(4)}\mathbf{r}^{B_4}\dot{\theta}^{(4)}) = 0, \tag{16, 17}$$

Here $\mathbf{T}_2^B = [-\sin\theta^{(3)} \quad \cos\theta^{(3)}]$ and $\mathbf{r}^{B_4} = [a \quad 0]^T$.

(5) *The revolute joint at* C:

$$\dot{\boldsymbol{\xi}}^{(1)} + \mathbf{T}_\theta^{(1)}\boldsymbol{\phi}^{C_1}\mathbf{B}^{1q}\mathbf{e}^{(1)}\dot{\theta}^{(1)} + \mathbf{T}^{(1)}\boldsymbol{\phi}^{C_1}\mathbf{B}^{1q}\boldsymbol{\chi}^{(1)}\dot{\boldsymbol{\eta}}^{(1)} - \dot{\boldsymbol{\xi}}^{(5)} = 0, \tag{18}$$

where $\boldsymbol{\phi}^{C_1}$ is the shape function of element q (which contains C_1) evaluated at C_1.

(6) *The prescribed motion of the piston*:

$$\mathbf{T}_1^B\dot{\boldsymbol{\xi}}^{(3)} = \mathbf{v}(t), \tag{19}$$

where $\mathbf{T}_1^B = [\cos\theta^{(3)} \quad \sin\theta^{(3)}]$ and $\mathbf{v}(t)$ is the prescribed piston velocity.

The boom is driven by a hydraulic actuator which is controlled by the operator. In general, throughout the motion, the hydraulic actuator is driven with constant velocity $\mathbf{v}_0$ so that the boom and piston oscillations are kept to a minimum level. Moreover, to avoid impact loading, the actuator velocity is increased from zero to $\mathbf{v}_0$ at the beginning of the motion and decreased from $\mathbf{v}_0$ to zero at the end of the motion which can be assumed cycloidal in time. This desired velocity profile is shown in Figure 4 and can be expressed as follows.

$$\mathbf{v}(t) = \begin{cases} \mathbf{v}_0 \dfrac{1}{t_1}\left[t - \dfrac{t_1}{2\pi}\sin\dfrac{2\pi}{t_1}t\right] & \text{for} \quad 0 \leqslant t \leqslant t_1 \\ \mathbf{v}_0 & \text{for} \quad t_1 < t < t_2 \\ \mathbf{v}_0 - \dfrac{\mathbf{v}_0}{(t_3 - t_2)}\left[(t - t_2) - \dfrac{(t_3 - t_2)}{2P}\sin\dfrac{2\pi(t - t_2)}{(t_3 - t_2)}\right] & \text{for} \quad t_2 \leqslant t \leqslant t_3 \end{cases} \tag{20}$$

If the pivots of Bodies 1 and 2 were at different points, the system would be a structure. The system is moveable owing to the special dimension obtained due to the concurrency of the pivots. Thus, the constraint equations written for Body 1 and Body 2 are linearly dependent. For this reason, one of the constraint equations is dropped to remove the linear dependency.

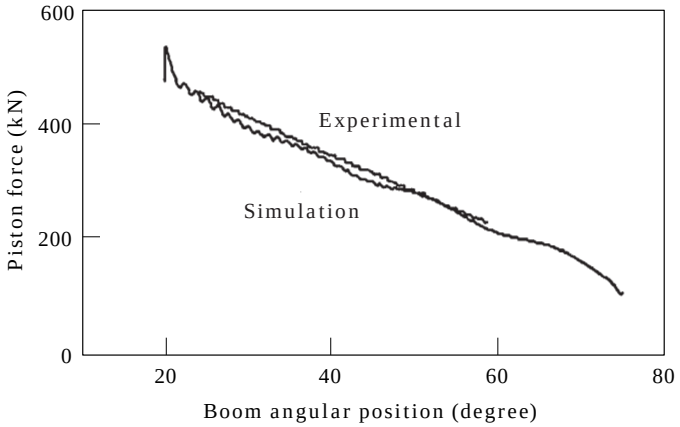

Figure 5. Piston force with respect to boom angular position (32·4 kN hook load and 30 s boom upward motion).

4. COMPUTER SIMULATION OF THE CRANE CHARACTERISTICS AND COMPARISON WITH THE EXPERIMENTAL RESULTS

Software has been developed for the analysis of the test crane. In this software, one can take any number of finite elements and modal variables for Body 1.

Experimental studies have been carried out by Balkan for the working range of the boom in which the boom was moved in 30 s [2]. This speed was selected in order to minimize the effect of flexibility. In that study, the pressure in the hydraulic actuator and the angular positions of the boom were measured. The oscillations in the pressure resulting from the boom oscillations are filtered out

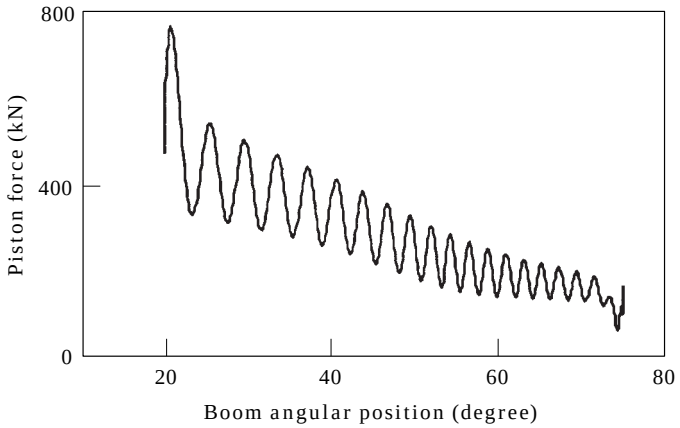

Figure 6. Piston force with respect to boom angular position (32·4 kN hook load and 10 s boom upward motion).

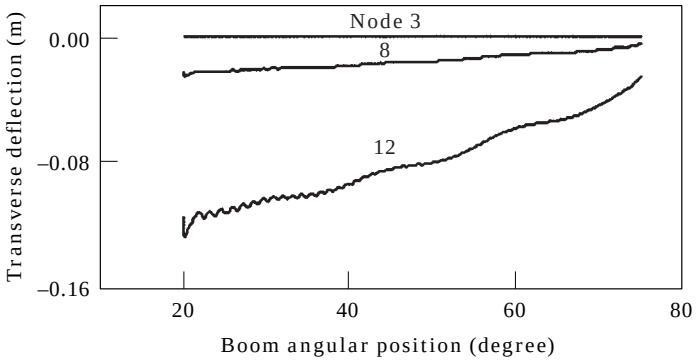

Figure 7. Transverse deflections of nodes 3, 8 and 13 with respect to boom angular position (32·4 kN hook load and 30 s boom upward motion).

in the control system, hence they are not seen in the measured data. The test crane was moved with a 32·4 kN hook load in the upward direction, and the variations of the pressures in the hydraulic actuator with respect to the boom angular positions are obtained for the 30 s motion of the boom. Therefore, the variations of the piston force with respect to the boom angular positions for the 30 s boom upward motion can be calculated for the 32·4 kN hook load.

The variations of the piston force with respect to the boom angular positions for the 32·4 kN hook load are simulated for the 30 s boom upward motion by using the computer code and given in Figure 5.

Experimental results for the 30 s motion of the boom are also shown in Figure 5. The data do not include piston acceleration and deceleration intervals. Moreover, since the boom oscillations are filtered out, they are not seen in the

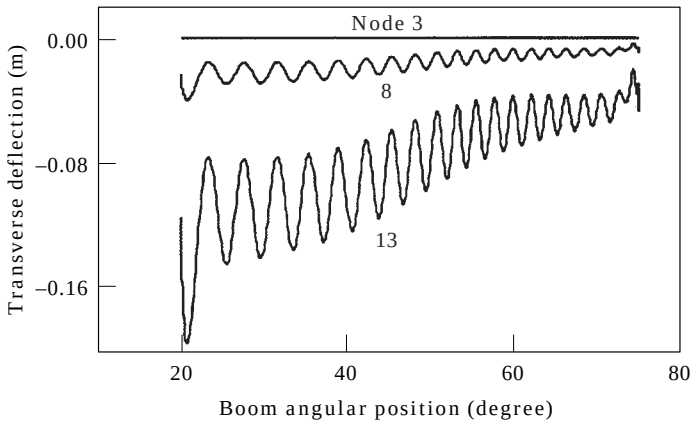

Figure 8. Transverse deflections of nodes 3, 8 and 13 with respect to boom angular position (32·4 kN hook load and 10 s boom upward motion).

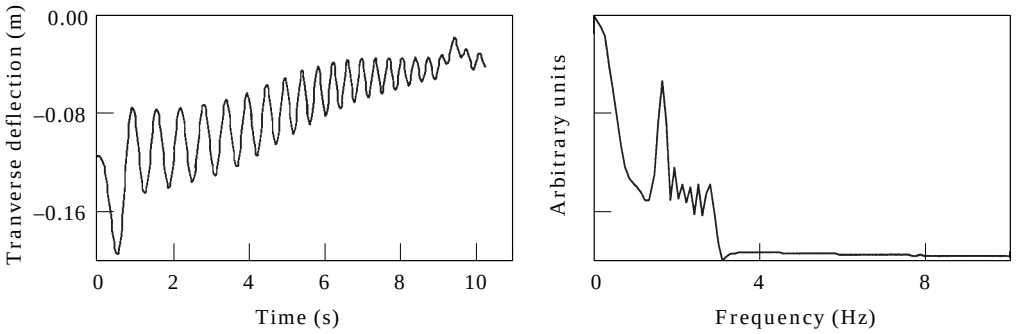

Figure 9. (a) Time response of transverse deflection of node 13. (b) FFT of transverse deflection of node 13.

figure. It is seen from the figure that simulation and experimental results for the 30 s boom motion are close to each other.

Similarly, the variations of the piston force with respect to the boom angular positions for the 32·4 kN hook load are simulated for the 10 s boom upward motion by using the computer code in order to make the effect of flexibility more significant as shown in Figure 6.

In the simulations, the boom is discretized by 12 finite elements. Two of them are taken on $\overline{A_0G}$ where the cross-sectional area is increasing from A_0 to G linearly and ten of them are taken on $\overline{GC}$ where the cross-sectional area is decreasing from G to C linearly. Damping is included for Body 1 by using a 2% damping ratio for the first two modes. It is assumed that the first 1·5 s is used for the acceleration and the last 1·5 s is used for the deceleration of the boom for the 30 s boom motion. In the case of 10 s boom motion, acceleration and deceleration intervals are assumed to be 1 s.

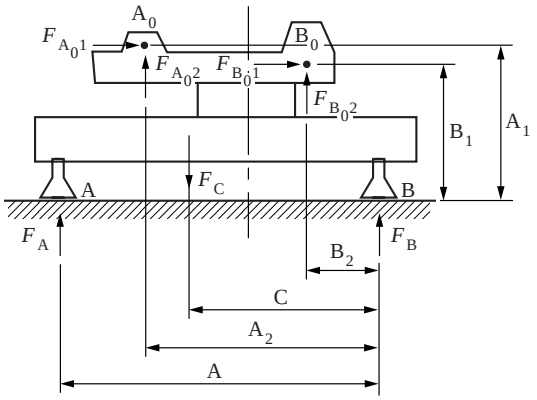

Figure 10. Free body diagram of the crane chassis. Dimensions in m: A 5·50; C 3·37; A_1 2·57; A_2 4·60; B_1 1·77; B_2 2·25.

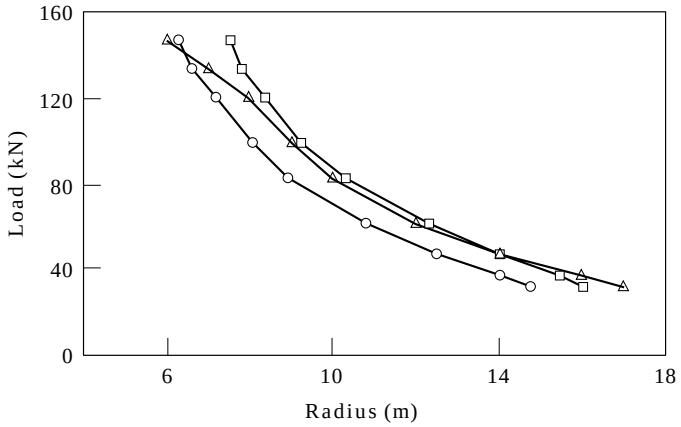

Figure 11. Lifting capacity on the hook. Key: —□—, simulation (30 s); —△—, manufacturer's data; —○—, simulation (10 s).

The transverse deflections of node 3, which is between the points A_0 and A of the boom, node 8, which is between the points A and C of the boom and node 13, corresponding to the tip point of the boom, C, are obtained with respect to the boom angular positions for both the 30 s and 10 s boom upward motion for the 32·4 kN hook load and are shown in Figures 7, 8, respectively. Since the magnitude of transverse deflections of node 3 is in the order of 10^{-5} m, the deflection of this node is not visible in the figures.

Figures 5–8 show that both the oscillation amplitudes and the mean values of the piston force and the transverse deflections of the nodes are greater for the 10 s boom motion compared to the 30 s boom motion. Hence, the effect of flexibility is seen clearly.

In all of the simulations, when the boom moves upward the piston force decreases, as expected. During the acceleration period of the piston, the piston force and the transverse deflection magnitudes and their respective oscillation amplitudes are larger than the values of the constant velocity interval. During the motion of the piston with constant velocity, the magnitudes of piston force and transverse deflection and their respective amplitudes decrease smoothly. During the deceleration of the piston, the magnitudes of piston force and transverse deflection decrease and their respective amplitudes increase. However, in the deceleration period, changes in magnitudes and amplitudes of the piston force and transverse deflection are smaller than the changes in acceleration period.

It is also seen from the simulations that there are two types of oscillations. The one with the small period is due to the boom oscillations and the one with the larger period is due to the load oscillations. The time response of the transverse vibration of the tip point (node 13) for 10 s boom upward motion and the 32·4 kN hook load is shown in Figure 9(a). The FFT magnitude plot of the data in Figure 9(a) is given in Figure 9(b).

The magnitudes at small frequencies correspond to the trend due to the excitation of the system. As the boom moves upwards, it goes towards the vertical position causing the boom transverse deflections to decrease. The frequency due to the load oscillations also falls into this frequency range. The frequencies over 1·5 Hz are due to the boom oscillations at its natural frequencies. The variation of the natural frequency with time is a characteristic of multibody systems and results in a chirp signal as seen in Figure 9(a).

5. SIMULATION OF THE LIFTING CAPACITY ON THE HOOK

Tipping simulation is performed in the blocked condition of the crane to see when tipping occurs as the boom moves in the upward and downward directions. When one of the reaction forces coming from the ground to the vertical jacks becomes zero, tipping occurs. Using the free body diagram of the crane chassis, shown in Figure 10, equation (21) is written for the tipping case as

$$F_{\mathrm{A}} = (1/\mathrm{A})(-F_{\mathrm{A}_01}\mathrm{A}_1 - F_{\mathrm{A}_02}\mathrm{A}_2 - F_{\mathrm{B}_01}\mathrm{B}_1 - F_{\mathrm{B}_02}\mathrm{B}_2 + F_{\mathrm{C}}\mathrm{C}) \tag{21}$$

where F_{A_01}, F_{A_02} and F_{B_01}, F_{B_02} are components of the reaction forces exerted by the boom and the cylinder on the crane chassis; F_{A} and F_{B} are the reaction forces exerted by the ground to the jacks and F_{C} is the body force of the crane chassis.

When F_{A} is smaller than or equal to zero, tipping condition occurs. For the 30 s and 10 s boom motions, the boom angular positions where F_{A} becomes zero are determined by using the developed software for different hook loads. The simulation results for the test crane are given in Figure 11. The allowable load specified by the manufacturer of the test crane is also shown in Figure 11 where radius is defined as the horizontal distance from the vertical axis of rotation of the crane to the tip of the boom at the tipping position, calculated as $R = 19{\cdot}5\cos\theta^{(1)} - 1{\cdot}83$ (m).

It can be seen from Figure 11 that when the boom motion time is decreased, the allowable load for the same radius decreases. Although there is no information about the conditions such as boom motion time while the allowable load data are being obtained, the plot of the allowable load is very similar to 30 s boom motion time simulation. In addition to this, it is noted by the manufacturer that these allowable load data should be used with a safety factor of 1·5.

6. CONCLUSION

In this study, the mobile crane characteristics are determined by using flexible multibody analysis. In order to achieve this goal software has been developed which is capable of carrying out dynamic analysis of the crane.

The coupled rigid and elastic motions of the system are formulated by using absolute co-ordinates and modal variables [3, 4]. Then, joint connections and prescribed motions are imposed as constraint equations. The flexible body is

modelled by the finite element method and the modal variables are used as the elastic variables by utilizing modal transformation.

The variations of piston force with respect to the boom angular positions for 32·4 kN hook load are simulated for both 30 s and 10 s boom upward motions by using the computer code for the velocity profile with cycloidal acceleration and deceleration. 30 s boom motion simulations are compared with the experimental results. Moreover, transverse deflections of node 3, node 8 and node 13 are obtained with respect to the boom angular positions for both 30 s and 10 s boom upward motion. Finally, load curves are generated for the 30 s motion and 10 s motion and compared with those of the manufacturer.

It is seen from the analysis that the boom motion time affects the crane dynamics considerably. For lower piston speeds (i.e., 30 s motion of the boom), the effect of flexibility is very small. Thus, the boom can be taken as a rigid body. However, when the piston speed is increased (i.e., 10 s motion of the boom), the effect of flexibility is dominant. The flexibility effect is seen in the simulations of the piston force and the lifting capacity on the hook for the 10 s boom motion.

It is also noted that the load curves determined here are for a cycloidal piston velocity profile which approximates the motion produced by an experienced operator. The load curves for other profiles can also be generated by the computer code developed. A profile that has discontinuities in the piston acceleration and deceleration would lower the lifting capacity considerably due to the larger deflections and inertia forces.

REFERENCES

1. K. Sato and Y. Sakawa 1988 *International Journal of Control* **48**, 2085–2105. Modelling and control of flexible rotary crane.
2. T. Balkan 1995 *Heavy Vehicle Systems, International Journal of Vehicle Design* **2**, 174–183. A moment limiter for mobile cranes.
3. A. A. Shabana 1985 *Journal of Vibration, Acoustics, Stress, and Reliability in Design* **11**, 431–439. Automated analysis of constrained systems of rigid and flexible bodies.
4. S. K. Ider 1991 *Computers and Structures* **40**, 939–945. Finite element based recursive formulation for real time dynamic simulation of flexible multibody systems.
5. Coles Crane Ltd. 1983 *Technical Data Sheet M*. 7347, Sunderland, England.